https://doi.org/10.46813/2025-158-050

SIMULATION OF A THERMIONIC CATHODE WITH INDUCTION HEATING

L.D. Pysarenko, I.L. Tsybulskyi
National Technical University of Ukraine "Igor Sikorsky Kyiv Polytechnic Institute", Kyiv, Ukraine
E-mail: i.tsybulskyy-ds31f@lll.kpi.ua

A numerical calculation of electron trajectories was carried out based on a hierarchical coupled model of cathode induction heating. The distribution of magnetic and electric fields generated by the inductor current was computed, which defines the boundary conditions for solving the total current equation and calculating current distribution in the device components. As a result, the temperature distribution within the cathode is established. The spatial distribution of physical properties within the cathode is taken into account in all energy conversion processes.

PACS: 29.25.Bx – Electron sources, 02.70.-c – Computational techniques; simulations

INTRODUCTION

Thermionic cathodes, being the core elements of vacuum and gas-discharge devices, remain subjects of research, development, and implementation [1 - 3]. Since the thermionic cathode in a vacuum tube is intended to emit electrons through heating, various methods of cathode heating are also being studied and developed. In addition to traditional directly heated and indirectly heated cathodes [4], designers have explored heating by means of inductors [5] and laser radiation [6, 7]. To increase emission current, microchannel cathodes are used [8]. In gas-discharge devices, plasma cathodes [9] are employed – sometimes referred to as virtual cathodes – but a metallic cathode is still required to initiate plasma generation.

The stable application domain of vacuum and gas-discharge devices is determined by their advantages over solid-state electronic devices:

- power density is two orders of magnitude higher;
- noise characteristics are two orders of magnitude lower;
- radiation resistance is several orders of magnitude greater.

These advantages have driven the development of high-power vacuum and gas-discharge devices, including measurement systems and equipment for specialized applications in the aerospace and defense industries. These include electron tubes [10], electron guns [11], microwave generators [12, 13], CRT displays [14], and X-ray sources [15]. The thermionic cathode remains a key component of electronic technology effectively used in complex engineering systems.

Induction heating (IH), which was previously used for cathode conditioning [10], allows the cathode to be electrically isolated from a grounded heating source while applying a high potential to it. This is essential for many technological and measurement devices [11, 15].

Laser heating also enables electrical isolation of the cathode from the heater, but it is inefficient due to energy conversion losses (electrical-optical-laser-thermal), with an efficiency of less than 1% [6, 7].

The traditional method of indirect heating of a thermionic cathode via thermal radiation through a layer of high-voltage insulation is also ineffective. The development of new electronic devices requires optimization of cathode geometry. Global experience with IH indicates broad design possibilities for cathodes using this method: cup-shaped, grid-type, and multi-lobed, multicell structures. IH allows tuning the current frequency for uniform heating of cathodes with various shapes.

In IH, electrons are affected both by the electrode potentials and the electromagnetic field of the inductor. Investigating this influence is the objective of the present study. The research was carried out by numerically calculating electron trajectories, based on a physical and topological model of the cathode assembly with induction heating.

1. MODELING OF INDUCTION HEATING

Modeling of induction heaters is actively applied across various industries: in metallurgy for optimizing billet heating prior to forging or rolling; in electronics for the development of induction heating systems used in soldering and heat treatment of components; and in medicine for designing induction-based hyperthermia and sterilization systems.

The numerical calculations are based on the finite element method (FEM), which is widely used for induction heating simulations due to its ability to accurately describe complex geometries and account for temperature-dependent material properties. Reference [16] presents the results of a three-dimensional FEM analysis that incorporates the temperature dependence of material characteristics.

When taking into account the interaction of various physical processes, multiphysics modeling based on physical-topological models is employed. In [17], an approach is described that combines electromagnetic and thermal modeling with experimental validation, providing high accuracy in predicting device characteristics.

Semi-analytical methods are also widely used to improve computational efficiency. In [18], a method is presented that combines initial FEM analysis with analytical equations, enabling faster simulations while maintaining accuracy.

2. MODEL OF A THERMIONIC CATHODE WITH INDUCTION HEATING

The calculation of the characteristics and parameters of any device is a complex task, as it requires the sequential solution of interrelated problems involving various physical phenomena. Such calculations are commonly referred to as multiphysics simulations. This approach is implemented through a physical-topological model that takes into account structural elements, defines the calculation sequence, and establishes the interrelations between physical processes.

Fig. 1 shows the physical-mathematical model used to calculate the characteristics of a cathode with an induction heater. The bottom row of the figure describes the functional purpose of each element in the model. The mathematical models are solved top-down, taking into account the initial conditions. The results of each stage are passed on to the subsequent mathematical model as its initial conditions. Feedback loops, shown as arrows, indicate the necessary adjustments to initial conditions related to the device geometry and the parameters of the supply voltage.

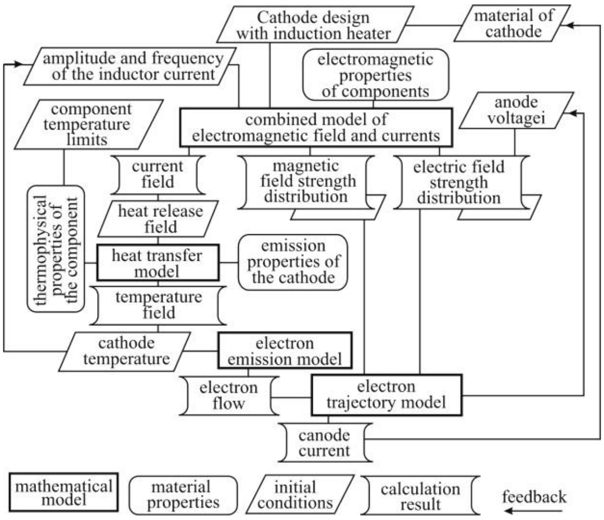

Fig. 1. Physico-topological model for calculating the characteristics

The presented physico-topological model encompasses mathematical models of four distinct physical processes:

- a combined electromagnetic field and current model;
- a heat transfer model for determining the temperature distribution within the cathode;
- a model describing electron emission from the cathode surface;
- a model of electron trajectories within the gap between the cathode and the anode.

Each mathematical model utilizes material parameters to define the coefficients within the governing mathematical equations, as well as initial conditions established by the design features of the device elements and their inherent physical properties.

The numerical computations yield spatial distributions of the relevant physical quantities within the elements of the device. These distributions serve as initial conditions for the subsequent mathematical model in the sequence. This stepwise approach continues until reaching the final model, which calculates the target device parameter. For the model under study, this parameter is the anode current, which can be employed as an optimization criterion for the device.

To change the initial conditions of the mathematical model, it is necessary to modify either the design or the parameters of the supply current.

The following sections consider the main mathematical models along with their initial conditions.

2.1. MATHEMATICAL MODEL OF CURRENT AND ELECTROMAGNETIC FIELD

The combined model of current and electromagnetic fields includes Maxwell's equations [19, 20] for calculating the electromagnetic field in vacuum based on the inductor current, followed by the calculation of currents in the cathode while considering the skin effect. Since the device has a symmetrical design, calculations using this model are more conveniently performed in cylindrical coordinates.

The electrical conductivity of metals is assumed to be independent of the direction and intensity of the electric field, related by Ohm's law: $j = \sigma E$. The magnetic properties of the materials are assumed linear, so the magnetic field varies sinusoidally in time. This assumption allows incorporating integral values of magnetic permeability and electrical conductivity of the components.

For the calculations, it is necessary to specify the electrical conductivity of the cathode and the inductor at operating temperatures. The analysis is simplified by representing the electrical currents as complex numbers: $z = z_0 \exp[i(\omega t + \varphi_z)]$, with a phase shift of 90° between the imaginary and real parts. Then, a linear combination of these complex quantities can represent an arbitrary phase angle. The complex quantity includes:

- the instantaneous value for the phase $\varphi_0 = -\omega \cdot t_0$,

$z_{\varphi 0} = \mathrm{Re}[z_0\, \mathrm{e}^{i(\varphi_z - \varphi_0)}] = z_0 \cos(\varphi_z - \varphi_0)$;

- amplitude value z_0;

- active value $z_R == \dfrac{\sqrt{2}}{2} z_0$.

The current in the inductor is defined as the sum of the electric current from an external source and the eddy current that induces a magnetic field in the vicinity of the cathode: $\mathbf{j} = \mathbf{j}_{\text{external}} + \mathbf{j}_{\text{eddy}}$.

The electromagnetic field is described by a partial differential equation with respect to the complex amplitude of the vector magnetic potential **A** (**B**=∇×**A**, **B** – magnetic flux density vector) [21]. In this case, the magnetic flux density vector **B** lies in the plane of the model (z0r), while the vector magnetic potential **A** and the electric current density vector **j** are orthogonal to that plane.

The components of the time-varying fields – j_θ and A_θ – are non-zero. If we denote these as *j* and *A*, and take into account that

$$B_z = \frac{1}{r}\frac{\partial (rA)}{\partial r} + \frac{\partial}{\partial z}\left(\frac{1}{\mu_r}\frac{\partial A}{\partial z}\right); \quad B_r = \frac{\partial A}{\partial z},$$

for the axisymmetric model, we have:

$$\frac{\partial}{\partial r}\left(\frac{1}{r\mu_z}\frac{\partial (rA)}{\partial r}\right) + \frac{\partial}{\partial z}\left(\frac{1}{\mu_r}\frac{\partial A}{\partial z}\right) - i\omega \cdot \gamma \cdot A = -j_{\text{eddy}},$$

where the components of the magnetic permeability tensor μ_z, μ_r, and electrical conductivity γ are constant in each element of the model. The current component j_{eddy} is inversely proportional to the radius (~1/*r*).

Up to the megahertz frequency of the electromagnetic field, the displacement current density affects the processes – we neglect it. That is, we do not take into account the component ∂**D**/∂t in Ampere's law $rot\mathbf{H} = \mathbf{j} + \frac{\partial \mathbf{D}}{\partial t}$. Then we have: $rot\mathbf{H} = \mathbf{j}$.

Model boundary conditions

At the boundaries of the calculation domains and on the axis of symmetry of the cathode, the Dirichlet condition is set with the value of the vector magnetic potential A_0 [19], which determines the absence of the normal induction component. The normal component of the magnetic induction vector on the cathode and inductor surfaces is also determined. The Dirichlet condition with axial symmetry is as follows: $r\mathbf{A}_0 = a + bzr + cr^2/2$, where a, b, and c are constants specific to each surface. In this case, the external field is defined by the normal component of the magnetic flux density at the boundary between the cathode and the crucible. The normal component of magnetic field induction on the cathode symmetry axis is equal to zero ($\mathbf{B}_n = 0$), i.e. a homogeneous Dirichlet condition is given.

The normal component of induction is $B_x = c\sin\alpha + b\cos\alpha$, where α is the angle of inclination of the surface to the z-axis.

The boundaries of the computational domain form a surface of magnetic antisymmetry, where homogeneous Neumann boundary conditions are applied: at the inner boundaries H $+t$ – H^{-t} = σ, where H_t is the tangential component of the magnetic field strength; at the outer boundaries H_t = σ, where σ is the linear density of the surface current. The "+" and "–" indexes indicate the areas to the left and right of the surface.

The values of the electrophysical and thermophysical parameters of the components are taken into account at the operating temperature corresponding to the specified electron emission.

The inductors are made of copper tubes for water cooling, which have high electrical conductivity. The operating temperature of the cooled inductors does not exceed 320 K.

Thermionic emission is described by the Richardson-Dushman equation:

$$J = AT^2 e^{-\frac{\varphi}{kT}},$$

where: J is the emission current density (A/m²); A = 120.173 A/(cm^2·K^2) is the universal emission constant, strongly dependent on the material and the state of the surface; T is the cathode temperature (K); φ is the work of electrons leaving metals (eV); k is the Boltzmann constant (k = 8.617·10^{-5} eV/K).

Table 1 shows the emission characteristics of cathode materials at operating temperature.

Tungsten cathodes possess high thermal stability, but require elevated temperatures for efficient emission due to their large work function. The addition of thorium reduces the work function, enabling high emission at lower temperatures.

Coating the cathode with barium or strontium oxides significantly lowers the work function, providing high emission at relatively low temperatures. Materials such as LaB_6 have a low work function and high stability, and are frequently used in electron microscopes and other devices.

Table 1

Physical parameters of cathode metals

Cathode Material	Output Operation, eV	Emission temperature, K	Emission constant, A/cm²·K²
Tungsten (W)	4.5	~2500	60
Molybdenum (Mo)	4.7	~2600	~3.1
Tantalum (Ta)	4.2	~2350	~0.6
Niobium (Nb)	4.2	~2150	~0.5
Thored W (Th-W)	2.63	~1700	3.0
Lanthanum Hexaboride (LaB_6)	2.66	~1800	29
Strontium Vanadate ($SrVO_3$)	~2.1	~1023	-
Barium oxide (BaO)	1.1	~1000	10^{-2}
Carbon Nanotubes	~4.5	~500	-

The addition of thorium or coatings of barium or strontium oxides reduces the work function, enabling high electron emission at lower temperatures. Lanthanum hexaboride (LaB_6) exhibits high stability. The perovskite $SrVO_3$ is a promising material for cathodes operating at low temperatures. Cathodes based on nanomaterials are used for field emitters due to the strong dependence of emission on the electric field strength.

Despite the variety of available cathode materials, high-power devices (above 10 kilowatts) use only refractory metals and dispenser cathodes based on them to ensure reliability, longevity, and stable emission.

Table 2 the characteristics of the most commonly used cathode materials are presented.

Table 2

Electrical conductivity of metals at operating temperature

Cathode Material	Electrical conductivity, ·10^6 S/m
Tungsten	1.35
Molybdenum (Mo)	18.7
Tantalum (Ta)	7.3
Niobium (Nb)	6.7
Thored W (Th-W)	5
Lanthanum hexa-boride (LaB_6)	~2
Strontium Vanadate ($SrVO_3$)	~0.1

Design values and characteristics

When studying devices with induction heating of the cathode, the following characteristics are determined:

1. Distribution of currents in the cathode.
2. Distribution of magnetic and electric field strength around the cathode and inductor.
3. To determine the temperature field, electrical losses as heat sources in the cathode (combined thermoelectric problem).

4. Inductor impedance to determine the efficiency of the design and operating mode of the device.

Fig. 2 shows an example of calculating the magnetic field strength in the vicinity of a cathode of a complex shape.

Due to limitations on the publication volume, the solution of the thermal problem is not presented in the paper. The result of this analysis is the temperature distribution across the cathode surface, which determines the emission current from the surface. Since emission currents of real cathodes strongly depend on the material, design, and surface condition (such as cathode activation), these parameters are typically accounted for empirically. This leads to noticeable discrepancies between simulation results and experimental data. Therefore, the authors deemed it appropriate to present the trajectories of electrons emitted by the cathode in the field of the inductor and collector (anode).

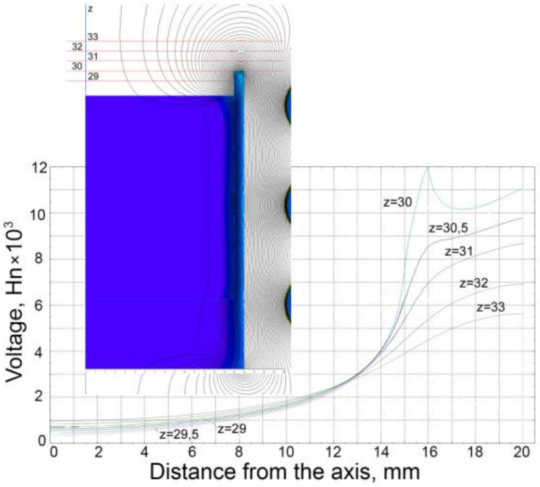

Fig. 2. Distribution of the magnetic field strength in the vicinity of the cathode of a complex shape

Although solving the induction heating (IH) problem for the cathode is important, the abundance of existing literature on IH and the limited scope of this publication compel the authors to omit the IH model and focus instead on the analysis of electron trajectories.

2.2. MATHEMATICAL MODEL OF THE ELECTRIC FIELD

Electric and magnetic fields act on an electron moving at a speed $\overline{V}$ with a force determined by the Lorentz formula:

$$\vec{F} = e\vec{E} + e[\overline{v}\vec{B}],$$

where e is the charge of the electron.

To determine the structure of the electric field, the equation of the electric potential φ was numerically solved

$$\nabla \cdot \left(\left[\varepsilon - \frac{i\gamma}{\omega} \right] \nabla \varphi \right) = 0, \qquad (1)$$

where γ is the electrical conductivity of the medium. Equation (1) is obtained by the joint solution of the Poisson equation for the electrostatic field ($\nabla \cdot \varepsilon \bar{\mathrm{E}} = \rho$), and the equation of current spreading in a conducting medium ($\nabla \cdot \bar{j} = -i\omega\rho$) taking into account Ohm's law (**j**=g**E**).

For an axisymmetric two-dimensional problem, equation (1) takes the form

$$\frac{1}{r}\frac{\partial}{\partial r}\left(\varepsilon_r r \frac{\partial \varphi}{\partial r} \right) + \frac{\partial}{\partial z}\left(\varepsilon_z \frac{\partial \varphi}{\partial z} \right) = -\rho,$$

where ε_z and ε_r are the elements of the tensor of the dielectric constant of the medium, which are constant within each element of the heater under study.

When calculating the problem, boundary conditions were set in the form of potentials of conductive surfaces (Dirichlet condition) (Fig. 3):

- at the boundary of the computational domain $\varphi_0 = 0$;

- at the upper turn of the inductor φ_I = 77.3 V, the voltage that ensures the heating of the cathode in the considered model to the operating temperature at a frequency of 440 kHz;

- at the middle turn of the inductor φ_I = 38.7 V, half voltage;

- on the lower coil of the inductor φ_I = 0.

An example calculation of the electric field structure with device components is shown in Fig. 3, where surface potentials and equipotential lines at 5 V intervals are presented.

There is no azimuth component of the field.

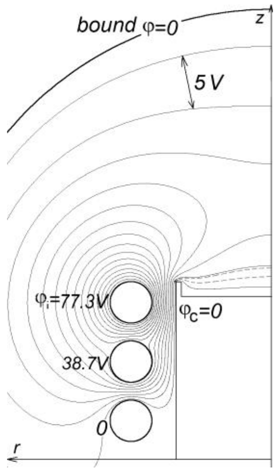

Fig. 3. Model of the electric field

2.3. ELECTRON TRAJECTORIES

To determine the trajectory of an electron in a nonuniform electric field, it is necessary to specify its mass, charge, initial velocity, and direction of emission from the surface. The emission angle is measured from the direction of the model's axis of symmetry. The angle between the emission direction and the plane of the model is assumed to be the same for all particles in the beam.

The following are determined as a result: the trajectory length, flight time, and the electron velocity at a point along the trajectory (marked with a cross on the trajectory map).

Electron trajectories are calculated based on the distribution of the electric field under the following assumptions:

- relativistic effects are not considered due to small accelerating voltages;

- the electrostatic field does not change (steady-state mode);

- within a finite element, the electrostatic field changes linearly;

- the influence of the electron space charge is not taken into account in the equation of motion (approximation of infinitely small current).

The trajectory ($x(t)$, $y(t)$, $z(t)$) of an electron in a two-dimensional electrostatic field $E(x,y)$ is described by Newton's system of differential equations:

$$\begin{cases} \dfrac{d^2x}{dt^2} = \dfrac{q}{m} E_x(x,y); \\ \dfrac{d^2y}{dt^2} = \dfrac{q}{m} E_y(x,y); \\ \dfrac{d^2z}{dt^2} = 0. \end{cases}$$

Equation determining the length $l(t)$ of the trajectory at time t:

$$\frac{dl}{dt} = \sqrt{\left(\frac{dx}{dt}\right)^2 + \left(\frac{dy}{dt}\right)^2 + \left(\frac{dz}{dt}\right)^2}\ .$$

Integration of the system of equations is performed using the Merson-Runge-Kutta numerical method: the step size is selected automatically; numerical integration stops immediately before the boundary of the finite element; in the last point inside the element, the trajectory is extrapolated using the first three terms of the Taylor expansion with respect to time. The resulting equation is solved using the Tartaglia-Cardano formula and takes into account the reduction of the equation order in uniform or zero fields.

In the calculations, electrons emitted by the cathode are assumed to have an average energy corresponding to the Maxwell distribution:

$$\frac{1}{2} m\bar{v}^2 = 2kT.$$

At a temperature of 2800 K, it will be

$$E = 7.728 \cdot 10^{-20}\ \text{J} = 0.483\ \text{eV}.$$

The average velocity of such electrons is:

$$\bar{v} = 2\sqrt{\frac{kT}{m}} = 4.119 \cdot 10^5\ [\text{m/s}].$$

At this speed, an electron in a vacuum will travel a distance $S = 5$ cm (reach the anode) in a time of

$$t = s / \bar{v} = 1.21 \cdot 10^{-7}\ \text{s}.$$

The half-life of the field oscillation at a frequency of 440 kHz is:

$$\tau = 1/2f = 1.136 \cdot 10^{-6}\ \text{s}.$$

During the positive half-period of the field, the electron manages to fly through the space of the device several times. In the negative half-cycle, electrons are limited by the field in the region of bulk charge near the cathode surface. Current ripple can be avoided by grounding the top coil of the inductor.

Fig. 4 shows examples of calculated trajectories Calculations were performed at the amplitude of the positive half-cycle of the inductor's electric field that ensures heating of the cathode to the operating temperature. Electron trajectories are shown for emission from various points on the surface at angles ranging from 0° to 85° relative to the surface normal. When the inductor has a negative potential, the electron trajectories are less curved.

Fig. 5 shows examples of calculated trajectories at an accelerating potential on a collector of 500 V. Electrons emitted from the inner cavity of the cathode are drawn into a beam to the anode.

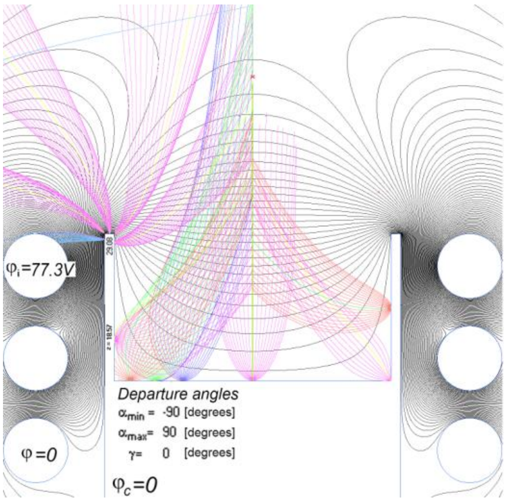

Fig. 4. Electron trajectories at different initial velocity vectors

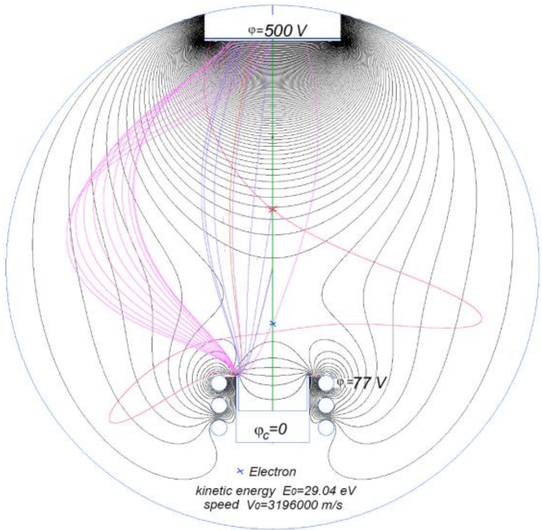

Fig. 5. Electron trajectories at an accelerating potential on a collector of 500 V

An insulator – either a glass or ceramic vacuum device housing – must be placed between the inductor and the cathode to prevent electron current from reaching the inductor. However, insulators can accumulate charges on their surfaces, creating parasitic fields and currents. To prevent these parasitic effects and to control electron trajectories, potential shields with longitudinal slits are used around the cathode, allowing the magnetic field to penetrate to the cathode.

CONCLUSIONS

The problem of analyzing electron trajectories emitted by a cathode with induction heating (IH) has been solved based on a physical-topological construction of a coupled model of the main processes. The combined model of induction currents and the electromagnetic field allowed determination of the current distribution in the inductor and cathode, as well as the structure of the magnetic and electric fields in their vicinity. Currents in the cathode define the temperature distribution over its surface and, accordingly, the electron emission. The structures of the magnetic and electric fields determine the electron trajectories.

The study of electron trajectories showed how the cathode shape controls the electron paths. The developed coupled model enables effective optimization of the design and operating modes of devices with IH cathodes.

Thus, the obtained data from the trajectory analysis laid the groundwork for the correct design of a device with IH at the next stage of practical implementation. Following this work, the testing of a new principle for constructing electron vacuum devices with an inductively heated thermionic cathode will be carried out.

Cathodes with IH open up broad prospects for use in high-power vacuum electronic devices without galvanic connection between the heating source and the cathode at high potential, as they potentially outperform contactless heating by laser or resistive heaters through a dielectric shell in terms of parameters.

REFERENCES

1. Gao, Jun-Yan, Yang, Yun-Fei, Zhang, Xiao-Ke, Li, Shi-Lei, Hu, Peng, Wang, Jin-Shu. A review on recent progress of thermionic cathode // *Tungsten (2).* 2020, № 3, p. 289-300. doi:10.1007/s42864-020-00059-1.
2. J. Wang, Y. Yang, Y. Wang, W. Liu, M. Zhou, T. Zuo. A review on scandia doped tungsten matrix scandate cathode // *Tungsten (1).* 2019, № 4, p. 191. doi:10.1007/s42864-019-00007-8.
3. D.M. Kirkwood, S.J. Gross, T.J. Balk, M.J. Beck, J. Booske, D. Busbaher. Frontiers in thermionic cathode research // *IEEE Trans Electron Devices*. 2018, p. 1-11. doi:10.1109/TED.2018.2804484.
4. J. Wang, M. Zhou, J. Liu. Advances in thermionic cathode of tungsten and molybdenum // *J. Rare. Met. (20).* 2001, № 3, p. 137.
5. S. Maikut, A. Kuzmichev, L. Tsybulskyi, N. Shynkarenko. The physico-topological simulation of a transmission X-ray tube with induction heating of the cathode // *Problems of Atomic Science and Technology*. 2023, № 4, p. 190-195. https://doi.org/10.46813/2023-146-190.
6. H.L. Andrews, A. Alexander, D.T. Beckman, A.S. Guider, M.A. Holloway, J.W. Lewellen, J.C. Moreno, G. Santana. A laser heated thermionic cathode // *XV th International Particle Accelerator Conference, Nashville, TN*, 2022. doi:10.18429/JACoW-IPAC2024-WFPC55.
7. M. Borland, B. Brajuskovic, R. Lindberg, N. Sereno. Pulsed laser heating of thermionic cathodes in rf guns // *Proceedings of Linear Accelerator Conference LINAC2010, Tsukuba, Japan.* 2010, p. 986-988.
8. J. Wiza. Microchannel plate detectors // *Nuclear Instruments and Methods (162)*. 1979, № 1, p. 587-601. doi:10.1016/0029-554X(79)90734-1.
9. A.S. An'shakov, A.V. Cherednichenko, V.A. Serikov, P.V. Domarov. Operating modes of vacuum plasmatrons with hollow cathodes // *IOP Conf. Series: Materials Science and Engineering.* 2019. doi:10.1088/1757-899X/560/1/012121.
10. Jerry Whitaker. *Power Vacuum Tubes. Handbook.* New York. "Springer Science+Business Media, LLC". (eBook). doi: 10.1007/978-1-4684-9987-2.
11. *Electronic gun for cathode ray tube.* Patent Japan JPH10116566A. https://patents.google.com/patent/JPH10116566A/en.
12. Weiye Xu. Review of the high-power vacuum tube microwave sources. [https://arxiv.org/abs/2003.04288]. https://doi.org/10.48550/arXiv.2003.04288.
13. Andre Haeff, Jack Copeland. The true history of the traveling wave tube // *IEEE Spectrum (52).* 2015, № 9. doi: 10.1109/MSPEC.2015.7226611.
14. K.I. Thoma, T. Dönges, M. Droba, O. Meusel, H. Podlech, K. Schulte-Urlichs. Tungsten electron emitter (te^2) with direct heated cathode by plasma stream // *13th Int. Particle Acc. Conf. IPAC2022*, Bangkok, Thailand, JACoW Publishing, 2022. doi:10.18429/JACoW-IPAC2022-MOPOMS018.
15. S. Chen, P. Wang. Thermionic enhanced heat transfer in x-ray tubes // *Applied Physics Letters (124).* 2024, № 1, p.1-10. doi:10.1063/5.0185921.
16. V.R. Nakum, N. Mehta. Research on induction heating a review // *International Journal of Science and Engineering Applications.* 2013, v. 2, № 6, p. 141-144. DOI:10.7753/IJSEA0206.1005.
17. M. Frivaldsky, M. Pavelek, T. Donic. Modeling and Experimental Verification of Induction Heating of Thin Molybdenum Sheets *// Applied Sciences (124).* 2021, № 1, p. 1-10. doi:10.3390/app11020647.
18. M. Areitioaurtena, U. Segurajauregi, V. Akujärvi, M. Fisk, I. Urresti, E. Ukar. A semi-analytical coupled simulation approach for induction heating // *Advanced Modeling and Simulation in Engineering Sciences*. 2021, № 14, p. 1-19.
19. A.E. Sluhockij, S.E. Ryskin. *Inductors for induction heating*. M.: "Energiya", 1974, 264 p.
20. V.S. Nemkov, V.B. Demidovich. *Theory and calculation of induction heating devices*. M.: "Energoatomizdat", 1988, 280 p.
21. J. Shackelford, W. Alexander. *Materials Science and Engineering Handbook*. Boca Raton: "CRC Press LLC". 2011, 1928 p.

Article received 10.06.2025

МОДЕЛЮВАННЯ ТЕРМОКАТОДА З ІНДУКЦІЙНИМ НАГРІВАННЯМ

Л.Д. Писаренко, І.Л. Цибульський

Чисельний розрахунок електронних траєкторій було проведено на основі ієрархічної зв'язаної моделі катодно-індукційного нагрівання. Було обчислено розподіл магнітних та електричних полів, які генеруються струмом індуктивності, що визначає граничні умови для розв'язання рівняння повного струму та розрахунку розподілу струму в компонентах пристрою. Встановлено розподіл температури всередині катода. Просторовий розподіл фізичних властивостей всередині катода враховується у всіх процесах перетворення енергії.